NEUROSCIENCE

Differential expression of voltage-gated sodium channels in afferent neurons renders selective neural block by ionic direct current

Fei Yang,[1,2]* Michael Anderson,[1]* Shaoqiu He,[1] Kimberly Stephens,[3] Yu Zheng,[4] Zhiyong Chen,[1] Srinivasa N. Raja,[1] Felix Aplin,[5] Yun Guan,[1,5†] Gene Fridman[4,6,7†]

The assertion that large-diameter nerve fibers have low thresholds and small-diameter fibers have high thresholds in response to electrical stimulation has been held in a nearly axiomatic regard in the field of neuromodulation and neuroprosthetics. In contrast to the short pulses used to evoke action potentials, long-duration ionic direct current has been shown to block neural activity. We propose that the main determinant of the neural sensitivity to direct current block is not the size of the axon but the types of voltage-gated sodium channels prevalent in its neural membrane. On the basis of the variants of voltage-gated sodium channels expressed in different types of neurons in the peripheral nerves, we hypothesized that the small-diameter nociceptive fibers could be preferentially blocked. We show the results of a computational model and in vivo neurophysiology experiments that offer experimental validation of this novel phenomenon.

INTRODUCTION

Electrical neuromodulation is an important modality to treat pain when pharmacologic interventions have been unsuccessful (*1*). Nociceptive information is transmitted from the periphery to the central nervous system (CNS) by thin myelinated Aδ fibers and unmyelinated, small-diameter C fibers (*2*). Electrical stimulation that suppresses "pain" signal conduction in peripheral nerves inhibits pain before these signals enter the CNS and diverge over multiple pathways. However, currently available neurostimulation therapies for pain have been associated with limited efficacy, short-lived pain inhibition, and undesirable side effects such as hypersensitivity to the changes in body positions and potential infections at the implant site, as well as at the electrodes implanted in the vulnerable position adjacent to the spinal cord (*3*–*5*).

These neurostimulation prostheses are fundamentally limited because they must use charge-balanced alternating current (AC) stimuli to avoid evolution of electrochemical reactions and liberation of toxic by-products at the electrode-tissue interface. Accordingly, they are typically designed to excite the neural tissue and are not efficient at inhibiting it. Inhibition would be desirable for pain treatment when peripheral and central sensory neurons develop increased excitability.

To attenuate neuron activity at low frequencies of up to 400 Hz, AC stimulation works indirectly by exciting CNS inhibitory interneurons that then inhibit target neurons. When delivered at a high frequency above 1.5 kHz, AC pulses hyperexcite neurons to engender adaptive changes that result in neuronal desensitization or conduction blockade on axons (for example, refractory state of sodium channels) (*6*). Although it can be effective, high-frequency depolarizing AC has a set of application-specific challenges for conduction block and pain inhibition. The onset of high-frequency stimulation can cause strong excitation of muscle efferent Aα fibers and non-nociceptive afferent Aβ fibers. This can lead to intense uncomfortable onset responses, muscle twitch, spasm, paresthesia, and, sometimes, allodynia after injury (*7*). In addition, high-frequency AC typically induces conduction block in low-threshold, large-diameter Aα/β fibers, but it is much less effective in suppressing the small-diameter nociceptive Aδ/C fibers (*8*).

Direct current (DC) delivered extracellularly is known to block the propagation of action potentials (APs) (*9*). Applications of DC for interfacing with the neural tissue, however, have been confined to laboratory studies and experimental short-term procedures because DC inherently violates safety charge injection criteria at the metal electrode–tissue interface. However, with the recent invention of safe direct current stimulation (SDCS) and the use of a modified separated interface nerve electrode, the possibility of using DC for neural interfacing in the form of an implantable prosthesis has emerged as a practical consideration. SDCS technology uses microfluidic valves to rectify the charge-balanced biphasic pulses delivered to metal electrodes within the implant to direct ionic current at the output of the device. SDCS thus offers the possibility of using a chronically implanted device to deliver ionic direct current (iDC) to block pain propagation (*10*).

To predict how iDC might affect different types of afferent sensory neurons, we first considered how AC electrical stimulation affects these neurons. Extracellularly delivered electrical pulses can alter the electrophysiological properties of large-diameter fibers at current amplitudes substantially lower than those needed to control small-diameter neurons (*11*). If this assertion were to hold true when delivering iDC blocking current instead of short pulses to the peripheral nerve, we would expect to preferentially suppress the large-caliber sensory fibers at relatively low amplitudes and only block the small nociceptive fibers as the amplitude of the stimulation current is increased. However, on the basis of the previously published neural modeling and electrophysiological findings, we hypothesized that the preferential effect on large- versus small-diameter fibers would actually be reversed when using cathodic (negative) iDC delivered to the peripheral nerve for an extended duration. If so, the delivery of cathodic iDC should preferentially suppress the small-diameter "pain" fibers while allowing the sensory information to propagate normally through the large-diameter neurons.

[1]Department of Anesthesiology and Critical Care Medicine, Johns Hopkins University, Baltimore, MD 21205, USA. [2]Department of Neurobiology, Capital Medical University, Beijing 100069, PR China. [3]Department of Pharmacology and Molecular Sciences, Johns Hopkins University, Baltimore, MD 21205, USA. [4]Department of Otolaryngology, Head and Neck Surgery, Johns Hopkins University, Baltimore, MD 21205, USA. [5]Department of Neurological Surgery, Johns Hopkins University, Baltimore, MD 21205, USA. [6]Department of Biomedical Engineering, Johns Hopkins University, Baltimore, MD 21205, USA. [7]Department of Electrical and Computer Engineering, Johns Hopkins University, Baltimore, MD 21205, USA.
*These authors contributed equally to this work.
†Corresponding author. Email: gfridma1@jhmi.edu (G.F.); yguan1@jhmi.edu (Y.G.)

iDC block modeling

The basis for the hypothesis that iDC block could have preferential suppression of small-diameter pain fibers is as follows: First, modeling results by Bhadra and Kilgore (*9*) using NEURON software suggest that long-duration current delivery requires similar current amplitude to block large- or small-diameter fibers. This effect is very different from the short-duration pulses that are well known to have a much stronger influence at any given current amplitude on the large-diameter axons. The model constructed by these investigators used the same voltage-gated channel models for large- and small-diameter neurons. Voltage-gated sodium channels (VGSCs) are important to the conduction and propagation of APs along the axons. Our second argument is that, on the basis of the differences in the electrophysiological response properties of the VGSCs expressed in the membranes of small- versus large-caliber neurons in peripheral nerves, we would expect cathodic iDC to block AP propagation in small-caliber fibers more efficiently than that in large-diameter axons.

Both cathodic (negative) iDC and anodic (positive) iDC delivered to an extracellular electrode have demonstrated the ability to block neural activity, albeit through different mechanisms. Whereas anodic extracellular iDC is the most intuitive method to block neural activity, by delivering a strong hyperpolarizing effect on the membrane potential, cathodic depolarizing iDC was shown to require substantially lower current amplitude to achieve neural block. Although the delivery of cathodic extracellular current depolarizes the neural membrane, its ability to achieve neural block is attributed to holding the VGSCs in their inactivated state and preventing them from recovering from inactivation. This mechanism driven by cathodic depolarizing iDC would prevent the sodium current from flowing into the cell to propagate the AP at the location of the block (*9*).

VGSCs involved in peripheral afferent signal propagation

Because cathodic iDC blocks neural activity by controlling the recovery from inactivation in VGSCs (*9*), the ability of the iDC at a given amplitude to block the propagation of an AP should depend on the electrophysiological properties of the particular variety of VGSCs present in the neuron's membrane. Ten varieties of VGSCs (Na_v 1.1 to Na_v 1.9 and Na_x) are currently known (*12*, *13*). They are preferentially expressed in different neuronal subtypes, as well as in different subdomains of a particular neural type throughout the nervous system. Because we are interested in blocking the AP propagation in the axons of the peripheral nerve, we needed to find the VGSCs that would be differentially present in the axons of the large- and small-caliber afferent neurons.

Specific to peripheral nerves, Na_v 1.1 and Na_v 1.6 are preferentially expressed in the membranes and nodes of Ranvier of the large-diameter sensory neurons (*14*, *15*), whereas Na_v 1.7, Na_v 1.8, and Na_v 1.9 dominate the VGSC expression in the small-diameter afferents (*16*). In these small-caliber fibers, Na_v 1.7 is preferentially expressed in nerve terminals (*17*) and in the C fiber axons (*18*). Na_v 1.8 is confined to the cell body and terminal arbor (*16*, *19*) and not in the axons of the fibers. Na_v 1.9 is expressed broadly in the nodes of Ranvier (*20*) of the small-caliber myelinated fibers. Because our modeling goal in this work was to investigate the hypothesis that the differences in VGSCs could give rise to the inverse recruitment of the fibers to iDC, we wanted to focus our examination on the large sensory Aβ fibers and compare their sensitivity to iDC block to that of the nociceptive C fibers. We therefore conducted a further review of the electrophysiological properties of Na_v 1.1, Na_v 1.6, and Na_v 1.7.

Na_v 1.1, Na_v 1.6, and Na_v 1.7 belong to a class of VGSCs called TTX-S, characterized by their sensitivity to tetrodotoxin, rapid activation, low thresholds, and rapid inactivation (*21*). Although both Na_v 1.1 and Na_v 1.6 are known to be expressed in the Aβ fibers, their relative contribution is unknown. However, only Na_v 1.6 is characterized by its inability to completely inactivate. Once inactivated, this channel retains a persistent Na^+ current at 10 to 20% of its original activated state (*22*). Accordingly, we postulate that this inability to completely inactivate could increase the amplitude required to hold a complete cathodic iDC block on large-caliber sensory fibers. In contrast, Na_v 1.7 is characterized by complete inactivation but very slow recovery from inactivation.

RESULTS

Model comparing small- versus large-diameter fiber membrane voltage in response to prolonged stimulation

To examine the stimulation effect on the membrane of a large- versus a small-diameter neuron, we used the extracellular stimulation cable model equations (*11*, *23*) implemented in MATLAB. We modeled the extracellular stimulation effect on the membrane potential of a small 1-μm unmyelinated fiber (like the nociceptive C fiber) and a large 10-μm-diameter myelinated fiber (like the non-nociceptive Aβ fiber) positioned at 1 mm from an extracellular electrode set to deliver −500 μA stimulation for 1 s. We recorded the change in membrane potential at 1 μs, 10 μs, 100 μs, 1 ms, 10 ms, 100 ms, and 1 s after stimulation onset. To focus on the size of the fibers alone rather than on the effect of the AP generation mechanism, we modeled the membranes at the initial state of −70 mV resting potential with no ion channels present in the membrane (Fig. 1). At 100 μs after stimulus onset, the simulation result agrees with the well-accepted notion that large-diameter neurons have a low threshold, whereas small-diameter fibers have a high threshold. The difference in the response of the two fibers to the same stimulus indicates that the large-caliber neuron is strongly depolarized, whereas the membrane of the small-caliber neuron is only slightly affected (Fig. 1A). This difference in membrane potential of the large- versus small-diameter fibers disappears, however, with prolonged stimulation. After the stimulus has been delivered for 1 s, the membrane potential of the two neurons is nearly identical (Fig. 1B). Our conclusion from this modeling effort is that, in contrast to the clear difference in thresholds to short pulses, the same amplitude stimulus affects large- and small-caliber neurons in the same way when the stimulus is delivered over long durations (Fig. 1C). This observation implies that any difference in the ability of the DC block to affect AP propagation must be attributable to factors other than the difference in axon diameters per se.

The second modeling experiment that we conducted used the same cable model as the one described above, but we also populated the axons with the computational models of voltage-gated potassium and sodium channels (*24*). We applied a cathodic iDC block at various amplitudes at 0 cm along the axon. In contrast to the case when no channels were present in the membrane, the membrane potential reached steady state within 100 ms of the block onset. This stabilization time is much shorter than the 1-s case presented earlier because the ion channels modeled in this membrane provide conductive ionic leakage currents in parallel with the capacitive transmembrane current, thereby lowering the membrane potential response time. Then, once the membrane potential reached steady state, we delivered a short 1-ms depolarizing pulse at −15 cm to test whether the DC block prevented the AP from propagating

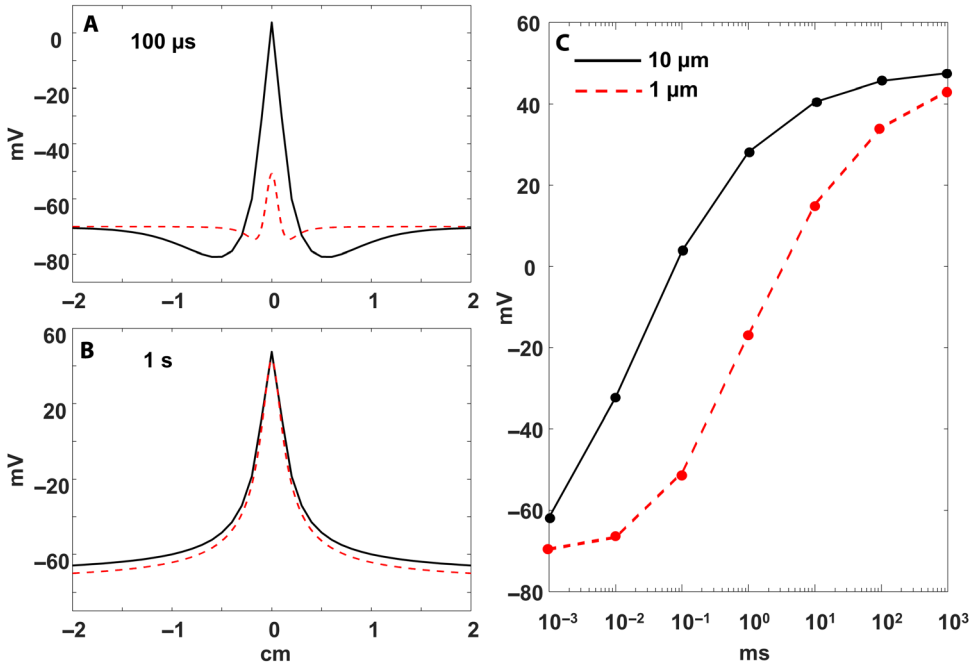

Fig. 1. Model of neural membrane responses of a 10-µm axon (like the Aβ sensory fiber) versus a small 1-µm axon (like the pain-carrying C fiber) to a −500-µA stimulus delivered at 1-mm distance at *x* = 0 cm for varying durations. (**A**) Membrane potential along the neuron of the two fibers after 100 µs of stimulation. (**B**) Membrane potential of the two fibers after 1 s of stimulation. (**C**) Maximum membrane voltage of the two fibers as a function of stimulus duration.

past it. The large-diameter myelinated fibers were populated with Na_v 1.6 sodium channel (*25*) and Hodgkin-Huxley (HH) potassium channel models with the standard approximation of 2.5-µm-long nodes of Ranvier separated by 1-mm-long myelin sheaths. The small unmyelinated fiber was populated with Na_v 1.7 (*25*) and HH potassium channel models. The models were otherwise identical in all regards in that they contained identical densities of potassium and sodium channels, as well as identical leakage conductivity in their membranes. They differed only in the types of sodium channel that were present in their membranes. The models were validated for their AP propagation speed and recovery rates. The large-diameter Aβ fiber AP propagation was 42 m/s (compared to the typical 30 to 80 m/s) with up to 120 spikes/s firing rate, whereas the small unmyelinated C fiber model propagated APs at an appropriate 1.8 m/s (compared to the typical range of 0.5 to 2 m/s) with up to 15 spikes/s firing rate, also appropriate for the C fibers.

As an example of the computational modeling exercise, the insufficient iDC amplitude block at 600-µA cathodic stimulation does not stop the AP from propagating, but a high enough amplitude at 900 µA does (Fig. 2A). As expected, the excitatory threshold for the Aβ fiber at 250 µA for a 500-µs pulse was much lower compared to the 3700-µA pulse needed to evoke AP in a C fiber (Fig. 2B, left). We then tested the ability of the fibers to block AP propagation. We observed that before we initiated the iDC block, at membrane resting potential, the steady state of the C fiber Na_v 1.7 channels was 97% inactivated with only 3% in a closed state. In contrast, the Na_v 1.6 channels of the Aβ fibers were 70% in the closed state with 30% inactivated. Therefore, cathodic block should be easier to establish and maintain with the Na_v 1.7 channels that are close to being completely inactivated at rest. Consistent with the hypothesis and this observation, we needed 670 µA to block the Aβ fibers, compared to only 290 µA needed to block the C fiber AP propagation (Fig. 2B, right).

In vivo examination of cathodic iDC block in rats

On the basis of the difference in channel dynamics and the predictions from the results of the membrane model, we hypothesized that cathodic iDC applied to the nerve might preferentially inhibit small-caliber nociceptive fibers. Therefore, we examined the effects of iDC on AP conduction in the sciatic nerve of an anesthetized rat preparation in which the distal end of the nerve was fully depolarized with a strong simulation pulse and the nerve blocking iDC current was delivered proximally. We extensively evaluated the ability of the iDC current to suppress AP propagation using three in vivo approaches. We assayed responses by recording compound action potential (CAP) in the nerve and by recording two features of spinal nociceptive transmission, namely, local field potential (LFP) and responses of wide dynamic range (WDR) neurons in the dorsal horn.

Cathodic iDC suppresses AP conduction in peripheral nerves

Using CAP recordings at the dorsal root, we first examined how cathodic iDC applied at the sciatic nerve broadly affects the conduction properties of peripheral Aα/β fibers and Aδ fibers in rats. We gradually increased iDC amplitude in a stepwise fashion (0.1 to 0.8 mA, 2 min per amplitude) and recorded the CAP evoked by a high-intensity test pulse (5 mA, 0.5 ms, biphasic, every 20 s) applied at the distal sciatic nerve before, during, and after iDC (Fig. 3A). The amplitudes of Aα/β and Aδ CAP were measured and normalized to pre-iDC baseline (Fig. 3B). This pattern of cathodic iDC decreased the amplitudes of CAPs mediated by myelinated Aα/β fibers and Aδ fibers with increasing iDC amplitude over time (n = 7; Fig. 3, B and C). The Aα/β CAP was significantly inhibited by 0.4 to 0.8 mA iDC, whereas Aδ CAP was significantly reduced by iDC at the lower amplitude of 0.2 mA (Fig. 3C). Furthermore, the Aδ CAP amplitude remained significantly lower than the pre-iDC baseline at 1 to 5 min after cessation of the highest iDC. However, Aα/β CAP quickly recovered to pre-iDC levels (Fig. 3C).

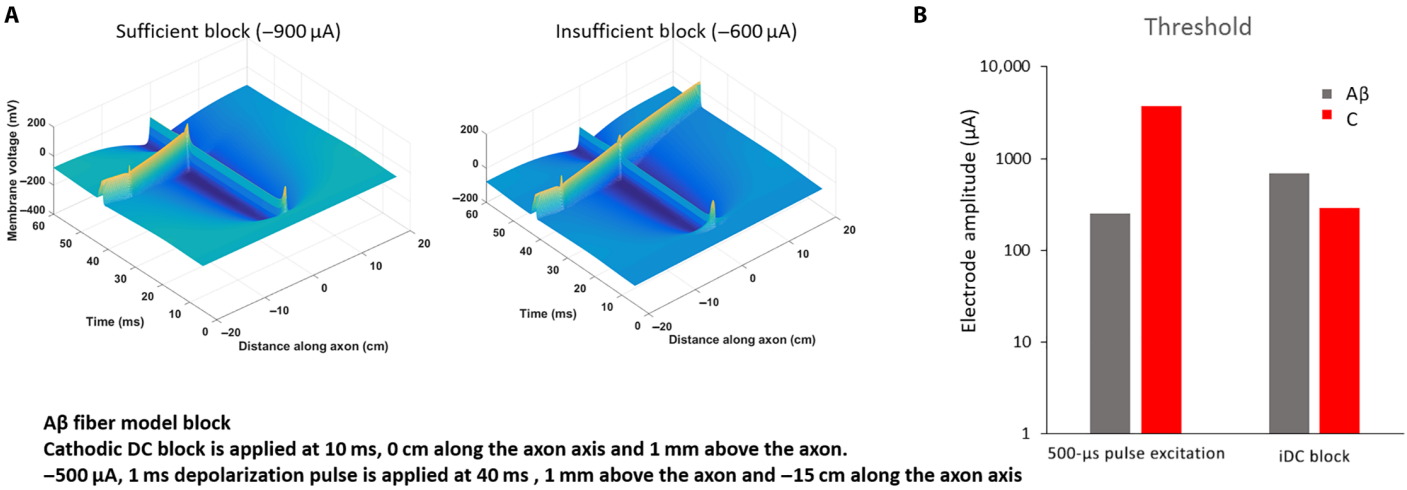

Fig. 2. Model of the AP block and the effect of two types of channels on the block threshold. (**A**) Model results showing the propagation of AP in the large 10-μm Aβ fiber model sufficiently blocked at 0 cm on the left and insufficiently blocked on the right. (**B**) Small-diameter unmyelinated axon (1 μm) and large-diameter myelinated axon (10 μm) are populated programmatically with the models of Na_v 1.7 or Na_v 1.6 VGSCs, respectively. Bars on the left show the stimulation threshold for a 500-μs pulse necessary to depolarize the 10-μm Aβ fiber (gray) versus the 1-μm unmyelinated C fiber (red). The bars on the right show the respective amplitude of the iDC necessary to block the propagation of AP in the Aβ versus the C fibers.

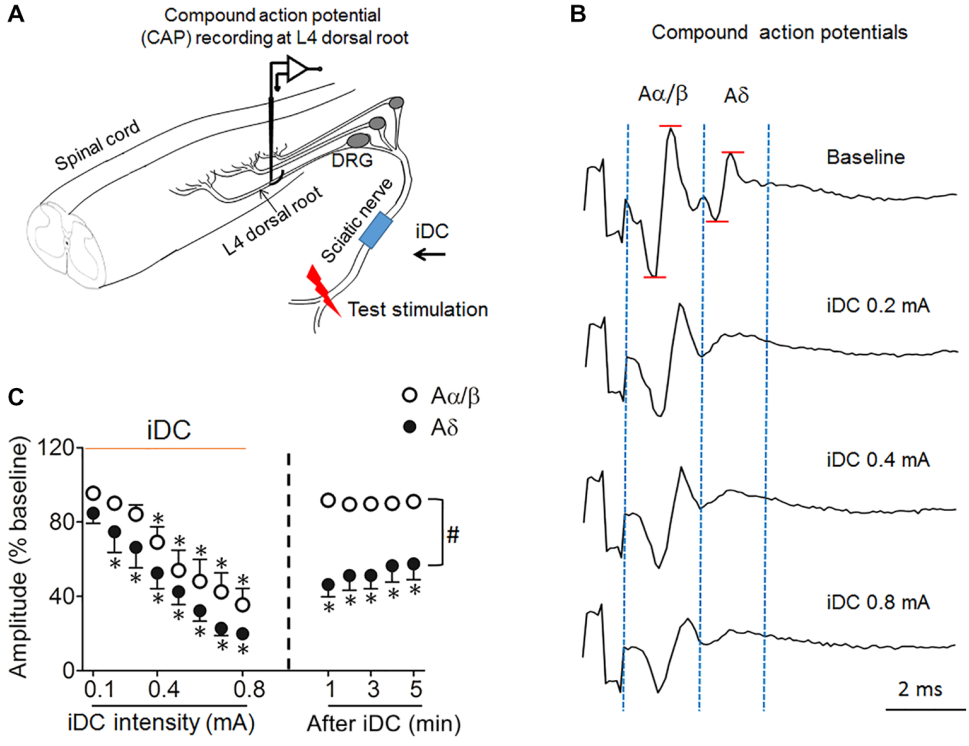

Fig. 3. Cathodic iDC at the sciatic nerve induces inhibition of AP conduction in the peripheral nerve. (**A**) Experimental setup for recording CAPs at the dorsal root in response to a test pulse (5 mA, 0.5 ms) applied at the distal sciatic nerve in rats. Monopolar cathodic iDC (0.1 to 0.8 mA, 2 min per amplitude) was applied to the sciatic nerve at mid-thigh level. DRG, dorsal root ganglion. (**B**) Examples of dorsal root CAPs evoked by the test stimulation before and after iDC stimulation. CAPs reveal two distinct groups of waves corresponding to Aα/β fiber and Aδ fiber activation. The amplitude of each CAP was measured from the positive peak to the negative peak of the waveform. (**C**) The amplitudes of Aα/β and Aδ CAPs decreased progressively as amplitudes of iDC stimulation increased (0.1 to 0.8 mA, 2 min per amplitude) and gradually recovered at 1 to 5 min after iDC stimulation. *$P < 0.05$ versus pre-iDC baseline; #$P < 0.05$ versus the indicated group at post-iDC, two-way repeated-measures analysis of variance (ANOVA) with Tukey post hoc test. Data are mean + SEM ($n = 7$).

Cathodic iDC inhibits broad nociceptive transmission in the dorsal horn

Because the conduction velocity (CV) of C fibers is slow and the conduction distance is long, the effects of iDC on AP conduction in small-diameter C fibers cannot be readily examined by dorsal root CAP assay. Small-diameter C fibers terminate principally at the superficial laminae (I to III) of the spinal dorsal horn (*26*). Spinal LFPs corresponding to C fiber (C-LFP) and to non-nociceptive Aα/β fiber (A-LFP) activation can be readily distinguished on the basis of activation threshold and CV. Therefore, we recorded spinal LFPs to examine changes in broad spinal

transmission of non-nociceptive and nociceptive inputs, as we applied intervening cathodic iDC at the sciatic nerve (Fig. 4A). The iDC protocol was the same as that in the study of CAP. We gradually increased iDC amplitude in a stepwise fashion (0.1 to 0.8 mA, 2 min per amplitude) and recorded the spinal LFP evoked by a high-intensity test pulse (25 V, 0.5 ms, biphasic) applied at the distal sciatic nerve before, during, and after iDC. The size of A-LFP (peak amplitude) and C-LFP (area under the waveform) was normalized to pre-iDC baseline (*27*). Cathodic iDC (2 min) produced a time-dependent inhibition of both A-LFP and C-LFP that increased with iDC amplitude (n = 8; Fig. 4, B and C). C-LFP was significantly inhibited by iDC at a lower amplitude than that needed to inhibit A-LFP (Fig. 4C). Furthermore, after the highest iDC was terminated, the C-LFP remained significantly decreased from the pre-iDC baseline for 2 min, but the reduction in A-LFP quickly reversed (Fig. 4C). These findings suggest that cathodic iDC may induce a preferential and longer inhibition of C-LFP over A-LFP.

Cathodic iDC preferentially inhibits C fiber–mediated responses in WDR neurons

Random neural activity cannot be readily examined in dorsal root CAP and spinal LFP assays because these methods are optimized to detect compound neuronal activity. WDR neurons are second-order neurons in the dorsal horn that receive convergent non-noxious (Aβ fiber) and noxious (Aδ, C fibers) inputs and play an important role in spinal pain processing (*28*, *29*). The number of APs in Aα/β, Aδ, and C components of WDR neurons can be separated in rats based on their latencies. Therefore, we conducted extracellular single-unit recording of WDR neurons in the deep dorsal horn (laminae III to V) to further examine whether cathodic iDC may differentially affect the transmission of inputs mediated by Aα/β, Aδ, and C fibers (Fig. 5A). WDR neuronal responses to a high-intensity test pulse (5 mA, 2 ms) applied at the cutaneous receptive field were recorded before, during, and 0 to 5 min after cessation of iDC (0.1 to 0.8 mA, 2 min per amplitude). The Aα/β, Aδ, and C components of WDR neurons were normalized to pre-iDC baseline. Cathodic iDC induced an intensity-dependent decrease in Aα/β, Aδ, and C components of WDR neurons in rats (n = 11; Fig. 5, B and C). Consistent with our hypothesis, the inhibition of the C component was significantly stronger than the inhibition of the Aα/β component during high-amplitude iDC in rats (Fig. 5C), suggesting that iDC might preferentially inhibit nociceptive transmission in WDR neurons. Furthermore, after the termination of iDC, the inhibition of the C component persisted for up to 5 min, but the Aα/β component quickly recovered to baseline (Fig. 5C).

DISCUSSION

We explored the potential for iDC to preferentially block small-diameter nociceptive fibers and allow larger-diameter fibers to propagate APs to

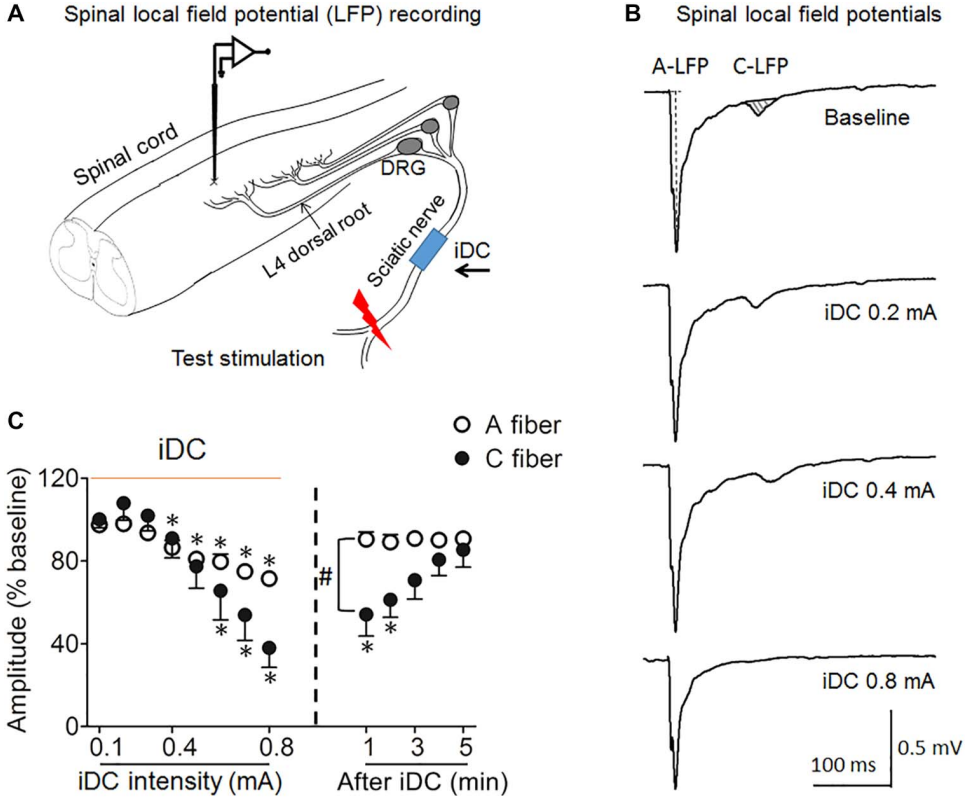

Fig. 4. Cathodic iDC at the sciatic nerve suppresses spinal LFP to peripheral test stimulation in an intensity-dependent manner. (**A**) Experimental setup for recording LFP from the superficial dorsal horn at the L4 spinal level to a test pulse (25 V, 0.5 ms) applied at the distal sciatic nerve in rats. Monopolar cathodic iDC stimulation was applied to the sciatic nerve at mid-thigh level. (**B**) Example traces show spinal LFP evoked by test stimulation before and after iDC stimulation. LFPs corresponding to A fiber and C fiber activation were distinguished on the basis of latency. The peak amplitude of A-LFP and area under the curve (AUC; shaded area) of C-LFP were measured off-line. (**C**) The amplitude of A-LFP and AUC of C-LFP decreased progressively as amplitudes of iDC increased (0.1 to 0.8 mA, 2 min per amplitude) and gradually recovered during the first 5 min after iDC cessation.*P < 0.05 versus pre-iDC baseline; $^{\#}P$ < 0.05 versus the indicated group at post-iDC, two-way repeated-measures ANOVA with Tukey post hoc test. Data are mean + SEM (n = 8).

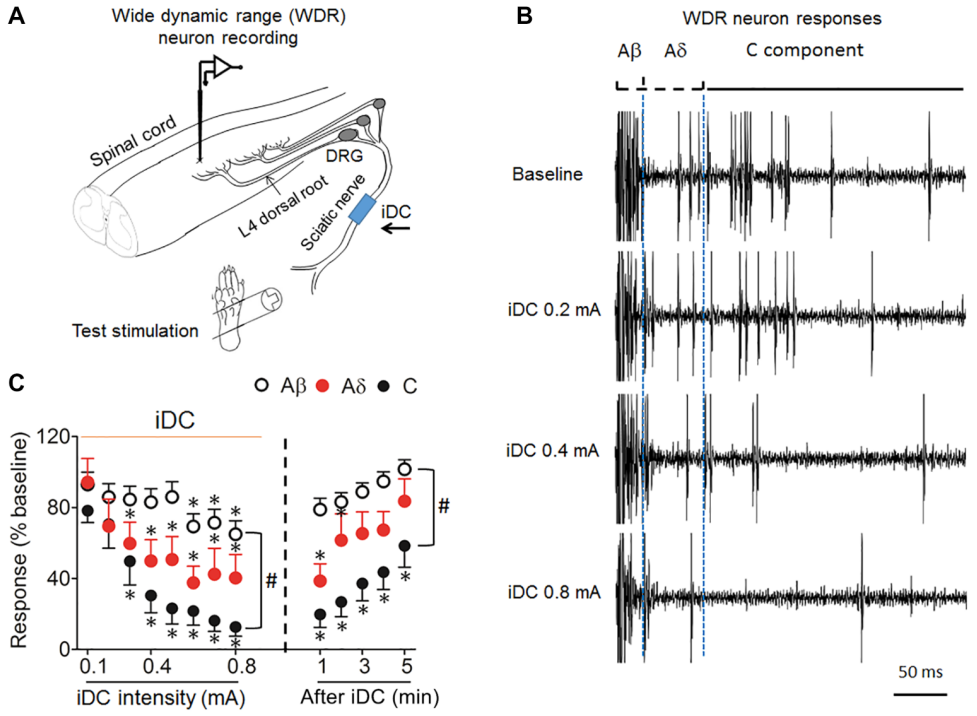

Fig. 5. Cathodic iDC at the sciatic nerve induces preferential inhibition of WDR neuronal responses to nociceptive afferent inputs. (**A**) Experimental setup for recording of WDR neurons from the dorsal horn to a test pulse (5 mA, 2 ms) applied to the hind paw of rats. Monopolar cathodic iDC stimulation (0.1 to 0.8 mA, 2 min per amplitude) was applied to the sciatic nerve at mid-thigh level. (**B**) Example of WDR neuron responses evoked by the test stimulation before and after iDC stimulation. WDR neuron responses can be divided into Aβ (0 to 25 ms), Aδ (25 to100 ms), and C (100 to 500 ms) components in rats based on the activation threshold and response latency. (**C**) The number of APs evoked in WDR neurons by test stimulation decreased as amplitudes of iDC increased (0.1 to 0.8 mA, 2 min per amplitude) and increased in the first 5 min after iDC stimulation ended. *$P < 0.05$ versus pre-iDC baseline; #$P < 0.05$ versus the indicated group at post-iDC; two-way repeated-measures ANOVA with Tukey post hoc test. Data are expressed as mean + SEM, $n = 11$.

conduct sensory information. Our modeling results suggest that the ability to create this preferential nociceptive block could be partially due to the type of VGSCs present in the membranes of large- versus small-diameter neurons. Together, the neurophysiological and modeling results offer exciting engineering possibilities for developing a "safe direct current stimulator"–type device (*10*, *30*) that could safely deliver ionic current for an extended duration as an alternative treatment option to control neuropathic pain.

A practical exploration path that follows from our present findings would be to define the effects of the iDC blocking mechanism on the overall pain pathway. Our investigation was limited to observing AP propagation at the periphery. The overall perception of pain is more complicated, and it depends on the circuits within the spinal cord where the interactions between the sensory and nociceptive pathways integrate in a nontrivial fashion. The effect of preferentially suppressing the small-caliber fibers on overall pain-related neurotransmission would need to be addressed through more thorough neurophysiological and behavioral studies.

Na_v 1.1 and Na_x are known to be expressed to some degree in the axons of the large Aβ neurons, and their contribution to signal transmission along the axon is not modeled here, where we focused on investigating the broad selectivity principle of iDC applied to VGSCs that were likely to contribute to the cathodic iDC block, namely, Na_v 1.6 and Na_v 1.7. In addition, although a wide range of voltage-gated potassium channel varieties are known to exist, we did not model their differences because we chose to focus our attention on the VGSCs that were strongly implicated (over the potassium channel dynamics) by

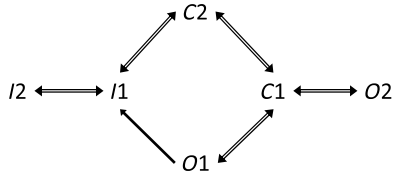

Fig. 6. Markov state transition model of the VGSCs. *I*1 and *I*2 are the inactivated states, *C*1 and *C*2 are closed states, and *O*1 and *O*2 are open states. Adapted with permission from Balbi *et al.* (*25*).

previous work on the iDC block (*9*). Further detailed and more accurate neural population models that contain the multiple types of voltage-gated channels in the correct densities and in the proper populations of neurons will allow the generation of highly concrete and testable hypotheses associated with using the iDC for pain suppression. Our goal in this work was to show that, in principle, the variability in VGSCs in the peripheral axons can introduce an inverse recruitment of neural block, and this is consistent with our experimental conclusions.

We believe that iDC represents a powerful complementary method of cybernetic communication with the nervous system. In contrast to using short pulses, this method can allow selective addressing of neurons based on their membrane channel dynamics rather than on their axon diameter. Independent of its use in neuropathic pain suppression, we believe that the results of our investigation provide a strong motivation and a direction for further exploration of the iDC neuromodulation methodology.

MATERIALS AND METHODS

Modeling

We used the standard computational implementation of the cable model to describe the effect of the extracellular stimulation on the membrane potential of an axon (*11*, *23*, *24*, *31*). We used HH-based equations and Markov models to simulate the voltage-gated currents in the axonal membrane (*11*, *24*). We conducted two sets of simulations in MATLAB. The first modeled the effect of the extracellular stimulation on a membrane that contained no ionic conductances to compare the effect of DC stimulation on the axons of different amplitudes per se. We then added the models of the voltage-gated sodium and potassium channels into the membranes of the simulated axons to determine the effect of these channels on neural block.

Extracellular neural stimulation model

Extracellular potential is described as a sum of superimposed electric fields in a homogeneous medium of extracellular resistivity ρ_e = 0.3 kilohm · cm in response to current $I_{e_i}(t)$ delivered from an electrode i placed above the axon positioned on the x axis, with its placement described as (x_i, z_i) in centimeters.

$$V_e(t) = \sum_{i=1}^{n} \frac{\rho_e I_{e_i}(t)}{4\pi\sqrt{x_i^2 + z_i^2}}$$

where n is the number of electrodes.

Membrane potential V_m was described in millivolts as a time-varying differential equation using the standard cable model. In the model, D is the diameter of the neuron, L is the length of the node of Ranvier in centimeters, and Δx is the length of the single myelin sheath in centimeters. The membrane had a capacity (c_m) of 1 μF/cm^2 , and internal resistivity (ρ_i) was equal to 0.03 kilohm · cm. For the myelinated fiber in our model, we assumed that $\Delta x = 100\,D$ and nodes or Ranvier were 2.5 μm, with L = 0.00025 cm. For the unmyelinated fiber, we assumed that $\Delta x = L$ = 0.01 cm.

$$\dot{V}_m = \frac{1}{c_m}\left(-I_{\text{ionic}} + \frac{D\Delta x}{4\rho_i L}\cdot\left(\frac{\partial^2 V_m}{\partial x^2} + \frac{\partial^2 V_e}{\partial x^2}\right)\right)$$

For the first simulation in which we wanted to observe the effect of cellular potential on the cellular membrane with no ionic channels, we set $I_{\text{ionic}} = 0$. We then ran the model for two fibers: a myelinated fiber (length, 40 cm) positioned with its center at $x = 0$ (for a 10-μm fiber, D = 0.0010 cm) and a 1-μm unmyelinated fiber (D = 0.0001 cm). For each, we delivered current from a single electrode driving −500 μA positioned 1 mm above the fiber at 0 cm along the membrane, that is, $n = 1$, $I_e = -500$, $x = 0$, and $z = 0.1$. We collected the simulated membrane potential V_m at 0.001, 0.01, 0.1, 1, 10, 100, and 1000 ms. We used a time step of dt = 0.001 ms for these simulations.

For the second experiment, we introduced ionic channels into the membrane, with $I_{\text{ionic}} = (I_{Na} + I_K + I_L)A_g$, where the current was represented per membrane surface area in microamperes per square centimeter. I_{ionic} was normalized to the membrane area of a 10-μm fiber and the 2.5-μm length of the node of Ranvier, with a surface area (A_{ranv}) of 0.001 cm(π)(0.00025 cm). For the 10-μm myelinated fiber, $A_g = 1$, and for the 1-μm unmyelinated fiber, $A_g = \frac{0.0001\ \text{cm}(\pi)(0.01\ \text{cm})}{A_{\text{ranv}}} = 4$.

Leakage current density

$$I_L = 0.01(V - 54.4)$$

Voltage-gated potassium channel

We implemented a standard HH potassium channel model.

$$V_k = -90.8\ \text{mV},\ g_k = 100$$

$$\alpha_n = \frac{0.01(V+55)}{1 - \left(e^{\frac{-(V+55)}{10}}\right)}$$

$$\beta_n = 0.125e^{\frac{-(V+65)}{80}}$$

$$\dot{n} = \alpha_n(1-n) - \beta_n n$$

$$I_K = g_K n^4 (V - V_K)$$

VGSC model

Because we formed our hypothesis around the behavior of the VGSCs, we used the models of all known VGSC channels unified in one dynamic Markov-type model recently published by Balbi *et al.* (*25*) (Fig. 6). This study describes the computational model with specific parameters for every known VGSC validated against the published electrophysiological data. For the model, we assumed that g_{na} = 300 and V_{Na} = 47.6.

$$I_{Na} = g_{na} X_o (V - V_{Na})$$

where X_o is the fraction of the open channels.

$$X_o = O1 + O2$$

$$\dot{C}1 = A_{I1C1}I1 + A_{C2C1}C2 - (A_{C1C2} + A_{C1I1})C1$$

$$\dot{C}2 = A_{C1C2}C1 + A_{O1C2}O1 + A_{O2C2}O2 - (A_{C2C1} + A_{C2O1} + A_{C2O2})C2$$

$$\dot{O}1 = A_{C2O1}C2 + A_{I1O1}I1 - (A_{O1C2} + A_{O1I1})O1$$

$$\dot{O}2 = A_{C2O2}C2 - A_{O2C2}O2$$

$$\dot{I}1 = A_{I2I1}I2 + A_{C1I1}C1 + A_{O1I1}O1 - (A_{I1C1} + A_{I1I2} + A_{I1O1})I1$$

$$\dot{I}2 = A_{I1I2}I1 - A_{I2I1}I2$$

$A_\omega = A_{s1s2}$ is the rate of state transition from state S1 to state S2.

$$A_\omega = B_h^\omega\left[1 + e^{\left(\frac{V - V_h^\omega}{K_h^\omega}\right)}\right]^{-1} + B_d^\omega\left[1 + e^{\left(\frac{V - V_d^\omega}{K_d^\omega}\right)}\right]^{-1}$$

Given the following definition for the function A that computes A_ω

$A_\omega = A(B_h, V_h, K_h, B_d, V_d, K_d, V)$
For Na_v 1.6:
$A_{C1C2} = A(0, 0, 0, 14, -8, -10, V)$
$A_{C2C1} = A(2, -38, 9, 14, -8, -10, V)$
$A_{C2O1} = A(0, 0, 0, 14, -18, -10, V)$
$A_{O1C2} = A(4, -48, 9, 14, -18, -10, V)$
$A_{C2O2} = A(0, 0, 0, 0.0001, -10, -8, V)$
$A_{O2C2} = A(0.0001, -55, 10, 0.0001, -20, -5, V)$
$A_{O1I1} = A(6, -40, 13, 10, 15, -18, V)$

$A_{I1O1} = A(0.00001, -40, 10, 0, 0, 0, V)$
$A_{I1C1} = A(0.1, -86, 9, 0, 0, 0, V)$
$A_{C1I1} = A(0, 0, 0, 0.08, -55, -12, V)$
$A_{I1I2} = A(0, 0, 0, 0.00022, -50, -5, V)$
$A_{I2I1} = A(0.0018, -90, 30, 0, 0, 0, V)$
and for Na_v 1.7:
$A_{C1C2} = A(0, 0, 0, 16, -18, -9, V)$
$A_{C2C1} = A(6, -48, 9, 16, -18, -9, V)$
$A_{C2O1} = A(0, 0, 0, 16, -23, -9, V)$
$A_{O1C2} = A(2, -53, 9, 16, -23, -9, V)$
$A_{C2O2} = A(0, 0, 0, 0.01, -35, -5, V)$
$A_{O2C2} = A(3, -75, 5, 0.01, -35, -5, V)$
$A_{O1I1} = A(4, -52, 12, 8, -27, -12, V)$
$A_{I1O1} = A(0.00001, -52, 10, 0, 0, 0, V)$
$A_{I1C1} = A(0.085, -110, 5, 0, 0, 0, V)$
$A_{C1I1} = A(0, 0, 0, 0.025, -55, -20, V)$
$A_{I1I2} = A(0, 0, 0, 0.00001, -80, -20, V)$
$A_{I2I1} = A(0.00001, -80, 20, 0, 0, 0, V)$

We modeled a 10-μm-diameter myelinated Aβ sensory fiber populated with the Na_v 1.6 model and then a 1-μm-diameter unmyelinated C fiber populated with the Na_v 1.7 model. We simulated AP propagation for each fiber and found the propagation speed, as well as the maximum firing rate, to ensure that the models produced reasonable estimates for each. For each simulation, we modeled a blocking iDC current delivered to an electrode positioned at $x = 0$ cm and $z = 0.1$ cm. Once the membrane current reached steady state (40 ms for the Aβ fiber and 80 ms for the C fiber), we added a 1-ms stimulation pulse delivered at $x = -15$ cm and $z = 0.01$ cm for the Aβ fiber and at $x = -1.5$ cm and $z = -0.01$ cm for the C fiber to depolarize the membrane. The AP then propagated toward both ends of the simulated membrane until it reached the 0-cm point at which it encountered the neural block. We iterated this simulation for each condition multiple times until we found the minimum block amplitude that could effectively stop the AP from continuing its propagation across the block. We also investigated the minimum amplitude of a 500-μs pulse needed to depolarize the membrane of the two fibers.

Animals

Adult male Sprague-Dawley rats (300 to 400 g; Harlan Bioproducts for Science) were used in electrophysiological recordings. Animals were housed under optimal laboratory conditions with a 12-hour light/dark cycle and free access to food and water. All procedures were approved by the Johns Hopkins University Animal Care and Use Committee (Baltimore, MD, USA) as consistent with the National Institutes of Health Guide for the Use of Experimental Animals to ensure minimal animal use and discomfort.

CAP recording at dorsal roots

CAPs were recorded at the L4 dorsal root by a metal hook electrode and were evoked by high-intensity test pulses (5 mA, 0.5 ms, biphasic) applied at the distal sciatic nerve in rats. CAP waveforms corresponding to Aα/β fiber and Aδ fiber activation were distinguished on the basis of the CV (*32*–*34*). The amplitude of CAP was measured from the positive peak to the negative peak of the waveform. Because of the long conduction distance and slow CVs in C fibers, C CAP could not be readily examined in the current setup.

Spinal LFP recording

We recorded LFP in the lumbar dorsal horn of rats under isoflurane anesthesia (1.5%) using an experimental setup similar to that described in our previous study (*27*). The dura overlying the recording segment (L4) was removed so that the fine tip of the tungsten recording microelectrode (1 milliohm at 1 kHz; Frederick Haer Company) would not be damaged as it was inserted into the dorsal horn. The LFP evoked by C fiber inputs (C-LFP) showed a long latency (90 to 130 ms) and high threshold to test stimulation (7 to 13 V, 0.5 ms) and was recorded at a depth ranging from 100 to 500 μm below the surface. A bandwidth of 1 to 300 Hz was used to remove artifacts without altering the C-LFP. A real-time, computer-based data acquisition and processing system (CED Spike 2) was used to collect analog data. Spinal LFP evoked by high-intensity test stimulation (25 V, 0.5 ms, 1 test per minute) at the sciatic nerve was examined 10 min before iDC (baseline), during iDC, and 0 to 10 min after iDC cessation.

Spinal WDR neuron recording

In anesthetized rats, we performed a tracheotomy, initiated mechanical ventilation, and made extracellular recordings of single dorsal horn neuronal activity as described in our previous studies (*32*, *33*). Briefly, a laminectomy was performed at vertebral levels T12 to L1 to expose the lumbar enlargements of spinal segments L3 to L5. During neurophysiological recording, animals were paralyzed with intraperitoneal pancuronium bromide (0.15 mg/kg; Elkins-Sinn Inc.) to facilitate controlled ventilation. We measured the activity of single neurons through extracellular recordings with fine-tip (<1.0 μm) Parylene-coated tungsten microelectrodes (3 milliohms at 1 kHz; Frederick Haer Company). Analog data were collected with a real-time, computer-based data acquisition and processing system (CED Spike 2). Deep WDR neurons were identified according to recording depths of 500 to 1000 μm, ranging from spinal laminae III to V (*28*, *32*). The evoked responses of WDR neurons to high-intensity electrical test stimuli (5 mA, 2 ms, biphasic, 1 test per minute) at the hind paw were examined before, during, and after iDC. The WDR neuronal responses were separated into different components according to activation thresholds and latencies: Aα/β (0 to 25 ms), Aδ (25 to 100 ms), and C (100 to 500 ms).

iDC stimulation

In general, DC cannot be used safely in implanted prostheses because the charge at the metal-saline interface causes tissue damage and electrode corrosion (*35*). To overcome this engineering challenge, we delivered continuous iDC by a constant current source (6221 DC and AC source; Keithley) to the sciatic nerve through microcatheter saline gel–filled DC catheters/tubes, with metal electrodes positioned far from the nerve to mimic safe DC stimulation delivery (*10*, *30*). The tip of the gel-filled DC tube (cathode) was placed in close contact with the nerve at mid-thigh level, with the return electrode (anode) placed in nearby muscle tissue. The sciatic nerve and electrodes were then covered with mineral oil.

Statistical analysis

No data were missing for any of the variables. The methods for statistical comparisons in each study are given in the figure legends. The sample size in each study was calculated on the basis of the respective statistical power analysis [power = 0.080, α = 0.05 (two-sided)] and previous similar studies (*27*, *34*, *36*). We randomized animals to different groups and used a blinded experimental design to reduce selection

and observation bias. STATISTICA 6.0 (StatSoft Inc.) was used for all statistical analyses. The Tukey honestly significant difference post hoc test was used to compare specific data points. Bonferroni correction was applied for multiple comparisons. Two-tailed tests were performed, and $P < 0.05$ was considered significant in all tests.

SUPPLEMENTARY MATERIALS

Supplementary material for this article is available at http://advances.sciencemag.org/cgi/content/full/4/4/eaaq1438/DC1

fig. S1. Example of a real-time output of the MATLAB script provided in the Supplementary Materials.

data file S1. iDCBlock.m MATLAB script that implements the model described in the publication.

REFERENCES AND NOTES

1. M. Gofeld, New horizons in neuromodulation. *Curr. Pain Headache Rep.* **18**, 397 (2014).
2. A. I. Basbaum, D. M. Bautista, G. Scherrer, D. Julius, Cellular and molecular mechanisms of pain. *Cell* **139**, 267–284 (2009).
3. B. A. Meyerson, B. Linderoth, Mode of action of spinal cord stimulation in neuropathic pain. *J. Pain Symptom Manage.* **31**, S6–S12 (2006).
4. J. W. Geurts, E. A. Joosten, M. van Kleef, Current status and future perspectives of spinal cord stimulation in treatment of chronic pain. *Pain* **158**, 771–774 (2017).
5. J. W. Geurts, H. Smits, M. A. Kemler, F. Brunner, A. G. H. Kessels, M. van Kleef, Spinal cord stimulation for complex regional pain syndrome type I: A prospective cohort study with long-term follow-up. *Neuromodulation* **16**, 523–529 (2013).
6. Y. Guan, Spinal cord stimulation: Neurophysiological and neurochemical mechanisms of action. *Curr. Pain Headache Rep.* **16**, 217–225 (2012).
7. L. J. Epstein, M. Palmieri, Managing chronic pain with spinal cord stimulation. *Mt. Sinai J. Med.* **79**, 123–132 (2012).
8. C. Tai, D. Guo, J. Wang, J. R. Roppolo, W. C. de Groat, Mechanism of conduction block in amphibian myelinated axon induced by biphasic electrical current at ultra-high frequency. *J. Comput. Neurosci.* **31**, 615–623 (2011).
9. N. Bhadra, K. L. Kilgore, Direct current electrical conduction block of peripheral nerve. *IEEE Trans. Neural Syst. Rehabil. Eng.* **12**, 313–324 (2004).
10. G. Y. Fridman, C. C. Della Santina, Safe direct current stimulation to expand capabilities of neural prostheses. *IEEE Trans. Neural Syst. Rehabil. Eng.* **21**, 319–328 (2013).
11. F. Rattay, *Electrical Nerve Stimulation, Theory, Experiments, and Applications* (Springer-Verlag/Wien, 1990).
12. N. Eijkelkamp, J. E. Linley, M. D. Baker, M. S. Minett, R. Cregg, R. Werdehausen, F. Rugiero, J. N. Wood, Neurological perspectives on voltage-gated sodium channels. *Brain* **135** (Pt. 9), 2585–2612 (2012).
13. A. L. Goldin, R. L. Barchi, J. H. Caldwell, F. Hofmann, J. R. Howe, J. C. Hunter, R. G. Kallen, G. Mandel, M. H. Meisler, Y. B. Netter, M. Noda, M. M. Tamkun, S. G. Waxman, J. N. Wood, W. A. Catterall, Nomenclature of voltage-gated sodium channels. *Neuron* **28**, 365–368 (2000).
14. J. A. Black, S. Dib-Hajj, K. McNabola, S. Jeste, M. A. Rizzo, J. D. Kocsis, S. G. Waxman, Spinal sensory neurons express multiple sodium channel alpha-subunit mRNAs. *Brain Res. Mol. Brain Res.* **43**, 117–131 (1996).
15. J. H. Caldwell, K. L. Schaller, R. S. Lasher, E. Peles, S. R. Levinson, Sodium channel $Na_v1.6$ is localized at nodes of ranvier, dendrites, and synapses. *Proc. Natl. Acad. Sci. U.S.A.* **97**, 5616–5620 (2000).
16. T. R. Cummins, P. L. Sheets, S. G. Waxman, The roles of sodium channels in nociception: Implications for mechanisms of pain. *Pain* **131**, 243–257 (2007).
17. J. J. Toledo-Aral, B. L. Moss, Z.-J. He, A. G. Koszowski, T. Whisenand, S. R. Levinson, J. J. Wolf, I. Silos-Santiago, S. Halegoua, G. Mandel, Identification of PN1, a predominant voltage-dependent sodium channel expressed principally in peripheral neurons. *Proc. Natl. Acad. Sci. U.S.A.* **94**, 1527–1532 (1997).
18. J. A. Black, N. Frézel, S. D. Dib-Hajj, S. G. Waxman, Expression of Nav1.7 in DRG neurons extends from peripheral terminals in the skin to central preterminal branches and terminals in the dorsal horn. *Mol. Pain* **8**, 82 (2012).
19. M. S. Gold, D. Weinreich, C.-S. Kim, R. Wang, J. Treanor, F. Porreca, J. Lai, Redistribution of $Na_V1.8$ in uninjured axons enables neuropathic pain. *J. Neurosci.* **23**, 158–166 (2003).
20. J. Fjell, P. Hjelmström, W. Hormuzdiar, M. Milenkovic, F. Aglieco, L. Tyrrell, S. Dib-Hajj, S. G. Waxman, J. A. Black, Localization of the tetrodotoxin-resistant sodium channel NaN in nociceptors. *Neuroreport* **11**, 199–202 (2000).
21. N. Ogata, H. Tatebayashi, Kinetic analysis of two types of Na+ channels in rat dorsal root ganglia. *J. Physiol.* **466**, 9–37 (1993).
22. Y. Chen, F. H. Yu, E. M. Sharp, D. Beacham, T. Scheuer, W. A. Catterall, Functional properties and differential neuromodulation of $Na_v1.6$ channels. *Mol. Cell. Neurosci.* **38**, 607–615 (2008).
23. F. Rattay, Analysis of models for extracellular fiber stimulation. *IEEE Trans. Biomed. Eng.* **36**, 676–682 (1989).
24. P. Dayan, L. F. Abbott, in *Theoretical Neuroscience* (MIT Press, ed. 1, 2001), pp. 166–176.
25. P. Balbi, P. Massobrio, J. Hellgren Kotaleski, A single Markov-type kinetic model accounting for the macroscopic currents of all human voltage-gated sodium channel isoforms. *PLOS Comput. Biol.* **13**, e1005737 (2017).
26. A. D. Sdrulla, Q. Xu, S.-Q. He, V. Tiwari, F. Yang, C. Zhang, B. Shu, R. Shechter, S. N. Raja, Y. Wang, X. Dong, Y. Guan, Electrical stimulation of low-threshold afferent fibers induces a prolonged synaptic depression in lamina II dorsal horn neurons to high-threshold afferent inputs in mice. *Pain* **156**, 1008–1017 (2015).
27. F. Yang, Q. Xu, B. Shu, V. Tiwari, S.-Q. He, L. P. Vera-Portocarrero, X. Dong, B. Linderoth, S. N. Raja, Y. Wang, Y. Guan, Activation of cannabinoid CB1 receptor contributes to suppression of spinal nociceptive transmission and inhibition of mechanical hypersensitivity by Aβ-fiber stimulation. *Pain* **157**, 2582–2593 (2016).
28. Y. Guan, J. Borzan, R. A. Meyer, S. N. Raja, Windup in dorsal horn neurons is modulated by endogenous spinal μ-opioid mechanisms. *J. Neurosci.* **26**, 4298–4307 (2006).
29. Y. Lu, H. Dong, Y. Gao, Y. Gong, Y. Ren, N. Gu, S. Zhou, N. Xia, Y.-Y. Sun, R.-R. Ji, L. Xiong, A feed-forward spinal cord glycinergic neural circuit gates mechanical allodynia. *J. Clin. Invest.* **123**, 4050–4062 (2013).
30. G. Y. Fridman, C. C. Della Santina, Safe direct current stimulator 2: Concept and design. *Conf. Proc. IEEE Eng. Med. Biol. Soc.* **2013**, 3126–3129 (2013).
31. F. Rattay, M. Aberham, Modeling axon membranes for functional electrical stimulation. *IEEE Trans. Biomed. Eng.* **40**, 1201–1209 (1993).
32. Y. Guan, P. W. Wacnik, F. Yang, A. F. Carteret, C.-Y. Chung, R. A. Meyer, S. N. Raja, Spinal cord stimulation-induced analgesia: Electrical stimulation of dorsal column and dorsal roots attenuates dorsal horn neuronal excitability in neuropathic rats. *Anesthesiology* **113**, 1392–1405 (2010).
33. F. Yang, Q. Xu, Y.-K. Cheong, R. Shechter, A. Sdrulla, S.-Q. He, V. Tiwari, X. Dong, P. W. Wacnik, R. Meyer, S. N. Raja, Y. Guan, Comparison of intensity-dependent inhibition of spinal wide-dynamic range neurons by dorsal column and peripheral nerve stimulation in a rat model of neuropathic pain. *Eur. J. Pain* **18**, 978–988 (2014).
34. F. Yang, A. F. Carteret, P. W. Wacnik, C.-Y. Chung, L. Xing, X. Dong, R. A. Meyer, S. N. Raja, Y. Guan, Bipolar spinal cord stimulation attenuates mechanical hypersensitivity at an intensity that activates a small portion of A-fiber afferents in spinal nerve-injured rats. *Neuroscience* **199**, 470–480 (2011).
35. D. R. Merrill, M. Bikson, J. G. R. Jefferys. Electrical stimulation of excitable tissue: Design of efficacious and safe protocols. *J. Neurosci. Methods* **141**, 171–198 (2005).
36. R. Shechter, F. Yang, Q. Xu, Y.-K. Cheong, S.-Q. He, A. Sdrulla, A. F. Carteret, P. W. Wacnik, X. Dong, R. A. Meyer, S. N. Raja, Y. Guan, Conventional and kilohertz-frequency spinal cord stimulation produces intensity- and frequency-dependent inhibition of mechanical hypersensitivity in a rat model of neuropathic pain. *Anesthesiology* **119**, 422–432 (2013).

Acknowledgments

Funding: This study was supported by an award from the Neurosurgery Pain Research Institute and the Blaustein Pain Fund at the Johns Hopkins University and by grants from the National Institutes of Health (Bethesda, MD, USA): R21NS099879 and R01NS070814 to Y.G. and R01NS092726 to G.F. This work was facilitated by the Pain Research Core funded by the Blaustein Pain Fund and the Neurosurgery Pain Research Institute at the Johns Hopkins University. **Author contributions:** F.Y., M.A., S.H., K.S., Y.Z., and Z.C. conducted the experimental work, analyzed the data, and prepared the figures. Y.G. and S.N.R. provided the resources and the oversight for the experimental work and statistical analysis. Modeling was conducted by G.F. and F.A. The manuscript was written by G.F. and Y.G. who contributed equally to its preparation. **Competing interests:** The authors declare that they have no competing interests. **Data and materials availability:** All data needed to evaluate the conclusions in the paper are present in the paper and/or the Supplementary Materials. Additional data related to this paper may be requested from the authors.

Submitted 5 October 2017
Accepted 21 February 2018
Published 11 April 2018
10.1126/sciadv.aaq1438

Citation: F. Yang, M. Anderson, S. He, K. Stephens, Y. Zheng, Z. Chen, S. N. Raja, F. Aplin, Y. Guan, G. Fridman, Differential expression of voltage-gated sodium channels in afferent neurons renders selective neural block by ionic direct current. *Sci. Adv.* **4**, eaaq1438 (2018).